Received: September 23, 2020. Revised: November 9, 2020. 340

International Journal of
Intelligent Engineering & Systems

http://www.inass.org/

The Effect of the Eigenvalues of the Zero-Forcing Detector on Its Performance in the Space-Division Multiplexing System

Ashraf Yahia Hassan[1]* **Ali Saleh[1]**

[1]*Benha Faculty of Engineering, Benha University, Egypt*
* Corresponding author's Email: ashraf.fahmy@bhit.bu.edu.eg

Abstract: Zero-Forcing (ZF) detector is used in Space-Division Multiplexing (SDM) receiver to remove interference among the received symbols. Previous works showed that the power of channel noise is enhanced in the output of the ZF detector. They recommend using the ZF detector when the received Signal-to-Noise Ratio (SNR) is high. This work proves that the performance of the ZF detector depends on the eigenvalues of the channel correlation matrix. The paper shows that if the sum of the eigenvalues of this correlation matrix is equal to the rank of the channel matrix, the ZF detector will not enhance noise power at its outputs. Moreover, if the sum of the eigenvalues is smaller than the rank of the channel matrix, the ZF detector will reduce noise power at its outputs. In this work, a theorem, which demonstrates the performance of the ZF detector in SDM receiver, is introduced and proved. The proposed work uses smart antennas in the transmitter and receiver to control the elements and eigenvalues of the channel matrix. The introduced theorem and a complete SDM receiver with ZF detector are simulated and evaluated at different conditions with different criteria. A real-time SDM receiver with ZF detector is also implemented and evaluated. The simulation and implementation results are shown at the end of this study. The results of the proposed systems show that a ZF detector can be used to remove interference in the SDM system without enhancing the channel noise.

Keywords: Space division multiplexing, Zero-forcing detector, Interference cancellation, Noise reduction, Eigenvalues, Correlation matrix.

1. Introduction

The multiplexing of symbols is used to increase the data transmission rate in communication systems. Multiplexing systems transmit *N* modulated symbols through *N* parallel channels in one symbol period. Frequency Division Multiplexing (FDM), Orthogonal Frequency Division Multiplexing (OFDM), Code Division Multiplexing (CDM), and Space Division Multiplexing (SDM) are the known multiplexing methods, which are used in communication systems to increase the data transmission rate. SDM is used to increase the bandwidth efficiency of the communication system as well as increasing the data transmission rate [1, 2]. The bandwidth efficiency is defined as the ratio between the total transmission rate and the total transmission bandwidth. In FDM systems, the maximum achievable bandwidth efficiency is half [3]. On the other hand, the bandwidth efficiency of OFDM systems is close to one but it never reaches it [4]. In SDM systems, the bandwidth efficiency is greater than one. The SDM transmitter sends *N* different modulated symbols parallel through the same frequency channel at the same time slot (symbol period) using *N* transmitting antennas [5, 6]. The transmitted symbols in the SDM system occupy the same bandwidth, which is used by the non-multiplexing system. Since the transmission rates from the *N* transmitting antennas are always equal, the total transmission rate in the SDM system is equal to the symbol rate of the non-multiplexed system multiplied by the number of the transmitting antennas. The bandwidth efficiency of the SDM system is also equal to the bandwidth efficiency of the non-multiplexed system multiplied by the number of the transmitting antennas. The SDM system has bandwidth efficiency greater than the bandwidth

efficiency of any other multiplexing systems. The SDM receiver must contain N receiving antennas to achieve the required transmission rate. Moreover, the channels between the transmitting antennas and the receiving antennas must be uncorrelated [7]. The rank of the channel matrix in the SDM system must be equal to the number of the transmitting antennas and the number of the receiving antennas. The rank of the channel matrix is also equal to the improvement factor in the transmission rate and bandwidth efficiency. The improvement in the transmission rate of the SDM system does not come without any cost. The transmitter and the receiver in the SDM system are more complex than the transmitters and the receivers in the other multiplexing systems.

The main disadvantage of multiplexing systems is the interference among the transmitted symbols. This interference is negligible in FDM systems because there is a guard band between the used frequency channels. However, in OFDM systems, the interference appears among the multiplexed symbols on the received subcarriers if there is a Doppler frequency shift in the transmission channel, or there is a miss-synchronization between the received subcarriers and the local subcarriers in the receiver [8,9]. In the CDM system, the interference among the multiplexed symbols appears when the used signature codes are not orthogonal [10]. As all multiplexing systems, the SDM system suffers from interference among the received symbols. The SDM system has the largest symbols interference among the multiplexing systems since the transmitted symbols from the N transmitting antennas have the same power and occupy the same bandwidth in the same time slot. Space-time codes are developed to prevent interference in SDM systems [11, 12]. However, these codes reduce the symbols transmission rate. This contradicts with the main objective of the multiplexing systems. The problem of symbols interference in multiplexing systems is directly proportional to bandwidth efficiency. Since the SDM system has the highest bandwidth efficiency, the interference in the SDM system is always larger than the interference in the other multiplexing systems. The receivers of the SDM systems must have interference cancellation detectors to eliminate or reduce the interference among the received symbols.

The interference cancellation detectors are classified into optimal interference cancellation detectors and suboptimal interference cancellation detectors [13,14]. The Maximum Likelihood (ML) detector is the optimal interference cancellation detector. It maximizes the likelihood function of the observation vector after the matched filters. The complexity of the ML detector is very high. The ML detector makes an exhaustive search for the most probably transmitted vector in a vector space of M^N vectors, where M is the number of the constellation symbols in the used modulation scheme and N is the number of the transmitting antennas [15]. The suboptimal interference cancellation detectors are proposed because their complexities are less than the complexity of the ML detector [16]. The suboptimal interference cancellation detectors are divided into three groups. The first group is the Parallel Interference Cancellation (PIC) detectors such as the Zero-Forcing (ZF) detector and the Minimum-Mean-Square Error (MMSE) detector. These detectors are linear. They remove the interferences among the N multiplexed symbols in the observation vector concurrently [17-19]. In ZF detection, the detector multiplies the observation vector by the inverse of the channel matrix. However, the MMSE detector multiplies the observation vector by the MMSE solution matrix, which minimizes the energy of the error between the desired symbols and the detected symbols. The second group of suboptimal detectors is the Successive Interference Cancellation (SIC) detectors. In these detectors, a decision is made about an interfering symbol in one stage, and then this symbol is subtracted from the other interfering symbols in the next stages. This process is repeated until all interfering symbols are detected [20, 21]. This procedure removes interferences if the decisions of the detected symbols in previous stages are correct; otherwise, it will duplicate the contribution of the interference. The last group of the suboptimal detectors is the Decision-Feedback (DF) detectors [22, 23]. These detectors are nonlinear. In DF detectors, a linear matrix maps the observation vector to the decision vector. This mapping removes a large amount of interference in the observation vector. A decision device is used to detect the symbols from the decision vector. These symbols are returned to the input of the decision device after remapping with another mapping matrix. The remapped vector is subtracted from the input of the decision device to remove the residual interference. The mapping matrices are chosen according to the MMSE criterion to minimize the error between the detected symbols and the desired symbols. The performance of the DF detectors is better than the performance of the linear detectors [24, 25]. However, the complexity of the DF detectors is higher than the complexity of the linear detectors.

In this paper, we concentrate on parallel interference cancellation using ZF detectors. The ZF detector has less computation complexity than the ML detector. The literature of communications says

that the ZF detector removes the interferences among the received symbols completely, but it enhances the channel noise at its output [16, 26-28]. Moreover, the ZF detector is very sensitive to the input Signal-to-Noise Ratio (SNR). The performance of the ZF detector is good at high input SNR and it is deteriorating at low SNR [16, 28-31]. This is the main disadvantage of the ZF detector and the reason for its suboptimal performance. However, in this work, it is proved that the performance of the ZF detector does not depend on the received SNR. However, it mainly depends on the sum of the eigenvalues of the channel correlation matrix. The paper will show that the noise power at the output of the ZF detectors varies at the same input SNR according to the sum of the eigenvalues of the channel correlation matrix. The proposed work will also show that the performance of the ZF detector can achieve performance closed to the performance of the ML detector and can outperform the MMSE detector if the channel matrix satisfies a certain condition.

The paper is organized as followed. In section 2, the mathematical models of the transmitted SDM signal and the received SDM signal are introduced. The used channel model is also represented in this section. Section 3 presents the eigenvalues theorem, which controls the performance of the ZF detector in different states. In section 4, an algorithm is introduced to control channel gain and channel matrix eigenvalues. Section 5 evaluates the eigenvalues theorem using MATLAB m-files. Different ZF detectors at different conditions are simulated and they are evaluated using different criteria according to the introduced eigenvalues theorem. A complete SDM receiver with ZF detector is also simulated and implemented using Xilinx FPGA kit to detect symbols from Rayleigh fading channel. Finally, the conclusions of the introduced study are represented.

2. The mathematical model of the received SDM signal

This section introduces the baseband transmitter and the baseband receiver of the SDM system. The transmitter of the SDM system is very simple. It consists of a baseband modulator, a serial-to-parallel converter, and N transmitting antennas. The baseband modulator converts binary symbols to complex modulated symbols according to the used modulation scheme. The serial-to-parallel converter arranges the modulated symbols into parallel vectors of N modulated symbols. The N transmitting antennas are used to transmit the modulated symbols in the parallel vectors. Each transmitting antenna transmits its corresponding modulated symbol in the parallel vectors. N also represents the multiplicative factor of the total symbol rate.

The symbol rate at the output of the baseband modulator in SDM transmitter is $N\times R_s$. R_s is the symbol rate at the output of the baseband modulator in the non-multiplexing system. In SDM transmitter, the parallel vectors of the modulated symbols are sent to the transmitting antennas with a rate of R_s vectors per second. The transmission rate of each transmitting antenna is R_s. The null-to-null bandwidth of the transmitted symbols is $2\times R_s$, which is the same as the bandwidth of the transmitted symbols in non-multiplexing system. Therefore, the SDM transmitter sends the modulated symbols with a rate of $N\times R_s$ in the same bandwidth of the non-multiplexing system. Eq. (1) shows the bandwidth efficiency of the SDM system (η_{SDM}) and its relation with the bandwidth efficiency of the non-multiplexing system (η_{NMS}).

$$\eta_{SDM} = \frac{Symbol\ rate}{Bandwidth} = \frac{NR_S}{2R_S} = \frac{N}{2} = N\eta_{NMS} \quad (1)$$

Eq. (2) represents the transmitted symbol by the n^{th} antenna in the m^{th} transmission period.

$$s_n(t - mT_s) = d_{(m-1)N+n}p(t - mT_s) \quad (m-1)T_s \le t \le mT_s \quad (2)$$

$d_{(m-1)N+n}$ is the modulated symbol, which is transmitted in the m^{th} transmission period by the n^{th} transmitting antenna. $p(t - mTs)$ is the normalized shaping pulse of the transmitted symbols. T_s is the period of one transmitted symbol. Fig. 1 (a) and 1 (b) show the block diagram of the SDM transmitter and receiver.

In the used SDM system, the transmitted symbols pass through Rayleigh flat fading channel. They are also corrupted with Additive-White Gaussian Noise (AWGN). The received symbols suffer from no Inter-Symbol Interference (ISI) if the channel is flat fading. When the fading channel is frequency selective, the received symbols suffer from ISI. To maintain the condition of flat fading, the bandwidth of the transmitted symbols is adjusted to be always smaller than the coherence bandwidth of the fading channel. In non-multiplexing systems, adjusting the symbols bandwidth to be smaller than the coherence bandwidth of the channel requires a reduction in the transmission rate. In the SDM system, the condition of flat fading is conserved at high transmission rates. This is accomplished by reducing the individual transmission rate (R_s) of each transmitting antenna to be smaller than half the coherence bandwidth of the

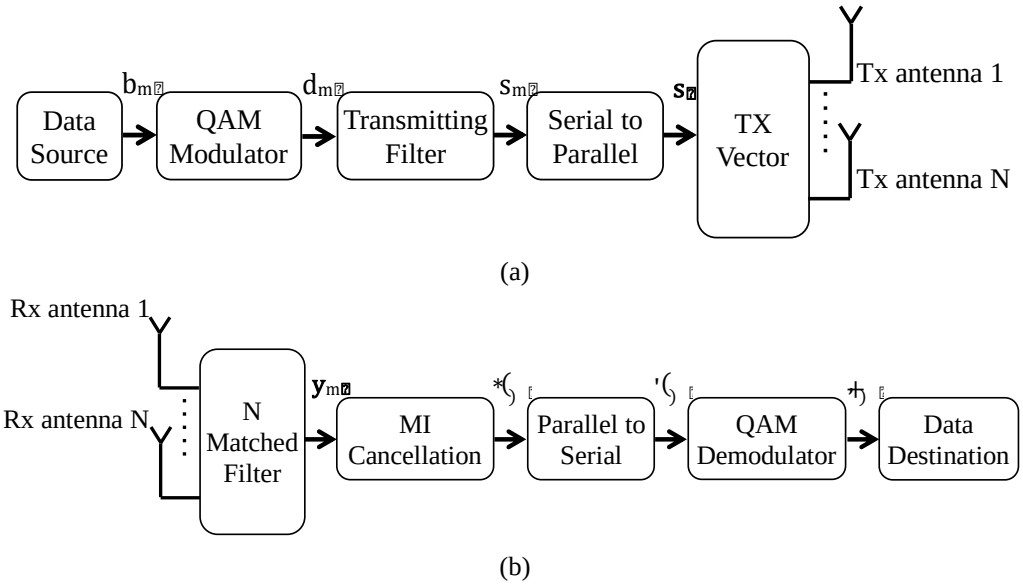

Figure. 1: (a) The block diagram of the SDM transmitter and (b) the block diagram of the SDM receiver

fading channel. However, increasing the number of transmitting antennas (*N*) keeps the total transmission rate high. This is similar to what happens in OFDM systems. The individual transmitting antennas play the same role as the subcarriers in OFDM systems. Hence, increasing the number of transmitting antennas is the cost, which should be paid by the SDM system to increase the symbol rate in flat fading channels.

To achieve the required symbols rate in the SDM system, the receiver must contain *N* receiving antennas. Moreover, the channel paths from the transmitting antennas to the receiving antennas must be uncorrelated. The spaces between the receiving antennas are adjusted to be multiple of the received signal wavelength to have uncorrelated paths from the transmitting antennas to the receiving antennas [7]. The fading channel between the transmitter and the receiver is assumed to be quasi-static. This means that the fading gain from each transmitting antenna to each receiving antenna is constant during the symbol period T_s, but it changes randomly from one symbol to another. Eq. (3) shows the received symbol $r_l(t - mT_s)$ by the l^{th} antenna at the m^{th} transmission period.

$$r_l(t - mT_s) = \sum_{n=1}^{N} \alpha_{ln} e^{-j\phi_{ln}} d_{(m-1)N+n} p(t - mT_s) + w_l(t) \quad (m-1)T_s \le t \le mT_s \quad (3)$$

α_{ln} is a Rayleigh random variable with $\sqrt{\frac{\pi}{2}}\sigma$ mean and $\left(2 - \frac{\pi}{2}\right)\sigma^2$ variance. ϕ_{ln} is a uniform random variable in the interval $[-\pi, \pi]$. The average power gain in the fading path from the n^{th} transmitting antennas to the l^{th} receiving antennas is $2\sigma^2$. $w_l(t)$ is a sample function of a white Gaussian noise process W(t) at the output of the l^{th} receiving antenna. The noise process has zero mean and σ_w^2 variance.

The output of each receiving antenna passes through a matched filter, which is matched to the shaping pulse of the received symbols. The output y_{lm} of the l^{th}-matched filter at the m^{th} symbol period is:

$$y_{lm} = \sum_{n=1}^{N} \alpha_{ln} e^{-j\phi_{ln}} d_{(m-1)N+n} + n_{lm} \quad (4)$$

n_{lm} is a zero-mean Gaussian random variable. It represents the noise random variable after the l^{th}-matched filter at the m^{th} symbol period. The outputs of the *N* matched filters at the m^{th} symbol period are arranged in one vector $\boldsymbol{y}_m$ as shown in Eq. (5).

$$\boldsymbol{y}_m = \boldsymbol{H}.\boldsymbol{d}_m + \boldsymbol{n}_m \quad (5)$$

$\boldsymbol{y}_m$ is the input observation vector to the interference cancellation detector. $\boldsymbol{H}$ is an $N \times N$ channel matrix. The elements of $\boldsymbol{H}$ are the fading gains from the transmitting antennas to the receiving antennas. The noise samples in $\boldsymbol{n_m}$ are independent identical distributed (*i.i.d*) random variables, because they come from independent sample functions of the Gaussian noise process *W*(t). The noise samples in $\boldsymbol{n_m}$ are Gaussian random variables with zero mean and σ_w^2 variance. A proper channel estimator is used to estimate the channel matrix $\boldsymbol{H}$ in the receiver. The channel estimation process is out of the scope of this paper. Thus, it is assumed that the receiver gets the Channel Status Information (CSI) from the channel estimator each symbol period.

According to Eq. (5), there are Multiplexing Interferences (MI) among the received symbols at the outputs of the matched filters. The ZF detector is used

to remove these interferences. It multiplies the observation vector in Eq. (5) by the inverse of the channel matrix $\boldsymbol{H}$. All previous works say that the mapping process done by the ZF detector enhances the channel noise power at its outputs. This is the reason for the suboptimal performance of the ZF detector. However, in this work, it is proved that the performance of the ZF detector is merely affected by the eigenvalues of the channel correlation matrix. As aforementioned, the performance of the ZF detector can achieve performance closed to the ML detector performance if the channel matrix satisfies a certain condition. In the following section, a theorem is introduced to determine the condition, which should be satisfied by the channel matrix and its inverse to remove the MI and to achieve a closed performance to the ML detector performance by the ZF detector.

3. The eigenvalues theorem for ZF detector

The output vector of the ZF detector is shown in Eq. (6). The ZF detector completely removes the MI among the received symbols. The elements of the output vector $\widehat{\boldsymbol{d}}_m$ are the estimations of the transmitted symbols in vector $\boldsymbol{d}_m$.

$$\widehat{\boldsymbol{d}}_m = \boldsymbol{H^{-1}}.\boldsymbol{y}_m = \boldsymbol{d}_m + \boldsymbol{H^{-1}}.\boldsymbol{n}_m \qquad (6)$$

The ZF detector will not increase the noise power at its output in Eq. (6) if the inverse of the channel matrix satisfies the following theorem.

Eigenvalues theorem

For independent-identical-distributed (i.i.d) input noise samples, the ZF detector does not increase the noise power at its output if and only if the summation of the average eigenvalues of the matrix $[\boldsymbol{H}^{-1}.(\boldsymbol{H}^{-1})^H]$ is smaller than or equal to the rank of the channel matrix.

$$\bar{P}_{ny} \le \bar{P}_{nx} \;\Leftrightarrow\; \sum_{n=1}^{N} E[\lambda_{\boldsymbol{n}}] \le N \qquad (7)$$

$\bar{P}_{nx}$ and $\bar{P}_{ny}$ are the average noise power at the input and the output of the ZF detector, respectively. $\lambda_{\boldsymbol{n}}$ is the n^{th} eigenvalue of the matrix $[\boldsymbol{H}^{-1}.(\boldsymbol{H}^{-1})^H]$.

Theorem proof

When a vector $\boldsymbol{x}$ of N random variables is linearly mapped with a full rank square complex matrix $\boldsymbol{A}$, the covariance matrix of the output vector $\boldsymbol{y}$ is equal to:

$$cov(\boldsymbol{y}) = \boldsymbol{A}\, cov(\boldsymbol{x})\boldsymbol{A}^H \qquad (8)$$

$(\,)^H$ is the Hermitian transpose of the matrix. The output vector $\boldsymbol{y}$ contains N correlated random variables. If the elements of vector $\boldsymbol{x}$ are i.i.d random variables with zero mean and σ_x^2 variance, the covariance matrix of vector $\boldsymbol{x}$ is the unity matrix multiplied by the variance σ_x^2. Hence, the covariance matrix of vector $\boldsymbol{y}$ is equal to:

$$cov(\boldsymbol{y}) = \sigma_x^2 \boldsymbol{A}\,\boldsymbol{A}^H \qquad (9)$$

The variance σ_x^2 represents the average power of each random variable in vector $\boldsymbol{x}$. The total average power in vector $\boldsymbol{x}$ is equal to $N\times\ \sigma_x^2$. The matrix $[\boldsymbol{A}\,\boldsymbol{A}^H]$ has N independent eigenvalues since matrix $\boldsymbol{A}$ is full rank. From Eq. (9), the eigenvalues of matrix $[cov(\boldsymbol{y})]$ are equal to the eigenvalues of matrix $[\boldsymbol{A}\,\boldsymbol{A}^H]$ multiplied with the variance σ_x^2 . Therefore, the eigenvalues of matrix $[\boldsymbol{A}\,\boldsymbol{A}^H]$ represent the power gain of the linear mapping process in the directions of its eigenvectors. Moreover, the eigenvalues of matrix $[cov(\boldsymbol{y})]$ represent the average power of the random variables in vector $\boldsymbol{y}$ in the directions of its eigenvectors. The total average power at the output of the linear mapping matrix $\boldsymbol{A}$ is the sum of the eigenvalues of matrix $[cov(\boldsymbol{y})]$. Since the random variables in vector $\boldsymbol{x}$ have the same average power (σ_x^2), the total average power $\bar{P}_{Ty}$ at the output of the linear mapping matrix $\boldsymbol{A}$ is:

$$\bar{P}_{Ty} = \sigma_x^2 \sum_n \lambda_n \qquad (10)$$

Here, λ_n is the n^{th} eigenvalue of matrix $[\boldsymbol{A}\,\boldsymbol{A}^H]$. If the sum of the eigenvalues of matrix $[\boldsymbol{A}\,\boldsymbol{A}^H]$ is equal to N, the total average power at the output of the linear mapping system will be the same as the total average power at its input. Moreover, if the sum of the eigenvalues of matrix $[\boldsymbol{A}\,\boldsymbol{A}^H]$ is less than N, the total average power at the output of the linear mapping system will be smaller than the total average power at its input. Therefore, for a vector $\boldsymbol{x}$ of i.i.d random variables, the total average power in the output of a linear mapping system to vector $\boldsymbol{x}$ is smaller than or equal to the total average power in vector $\boldsymbol{x}$, if and only if the sum of the eigenvalues of the product of the mapping matrix with its Hermitian transposed is smaller than or equal to the rank of the mapping matrix.

If the mapping matrix $\boldsymbol{A}$ is a random matrix, the covariance matrix in Eq. (9) is random too. The average covariance matrix $\bar{\boldsymbol{\Phi}}_{\boldsymbol{y}}$ of vector $\boldsymbol{y}$ is equal to:

$$\bar{\boldsymbol{\Phi}}_{\boldsymbol{y}} = E[cov(\boldsymbol{y})] = \sigma_x^2 E[\boldsymbol{A}\,\boldsymbol{A}^H] \qquad (11)$$

$E[\boldsymbol{A}\,\boldsymbol{A}^H]$ is the correlation matrix of the random mapping matrix $\boldsymbol{A}$. The eigenvalues of the correlation matrix $E[\boldsymbol{A}\,\boldsymbol{A}^H]$ represent the average power gains of the random mapping system $\boldsymbol{A}$ in the directions of its eigenvectors. In this case, the total average power at the output of the mapping system $\boldsymbol{A}$ is:

$$\bar{P}_{Ty} = \sigma_x^2 \sum_n \grave{\lambda}_n \tag{12}$$

$\grave{\lambda}_n$ is the n^{th} eigenvalue of the correlation matrix $E[\boldsymbol{A}\,\boldsymbol{A}^H]$. Since the trace of the correlation matrix $E[\boldsymbol{A}\,\boldsymbol{A}^H]$ is equal to the average of the trace of the random matrix $[\boldsymbol{A}\,\boldsymbol{A}^H]$, the sum of the eigenvalues of the correlation matrix $E[\boldsymbol{A}\,\boldsymbol{A}^H]$ is equal to the sum of the average of the random eigenvalues of matrix $[\boldsymbol{A}\,\boldsymbol{A}^H]$. Eq. (13) shows the mathematical proof of the previous statement.

$$tr\big[E[\boldsymbol{A}\,\boldsymbol{A}^H]\big] = \sum_n E\big[\boldsymbol{D}_{\boldsymbol{A},n}\big] = E\big[\sum_n \boldsymbol{D}_{\boldsymbol{A},n}\big] = E[\sum_n \lambda_n] = \sum_n E[\lambda_n] \tag{13}$$

$\boldsymbol{D}_{\boldsymbol{A},n}$ is the n^{th} diagonal element of the matrix $[\boldsymbol{A}\,\boldsymbol{A}^H]$. Therefore, Eq. (12) can be rewritten as shown in Eq. (14).

$$\bar{P}_{Ty} = \sigma_x^2 \sum_n E[\lambda_n] \tag{14}$$

Eq. (14) says that the total average power at the output of a random linear system is equal to the summation of the average eigenvalues of the random matrix $[\boldsymbol{A}\,\boldsymbol{A}^H]$ multiplied with the variance σ_x^2. Hence, the average power $\bar{P}_{Ty}$ at the output of a linear mapping process is smaller than or equal to the average power at its input $\bar{P}_{Tx}$ if the summation of the averages of the eigenvalues of the random matrix $[\boldsymbol{A}\,\boldsymbol{A}^H]$ is smaller than the rank of the $\boldsymbol{A}$. This completes the proof of the eigenvalues' theorem. □

Now, the eigenvalues theorem is applied on the ZF detector. The ZF detector uses the inverse channel matrix $\boldsymbol{H}^{-1}$ to map the noise vector $\boldsymbol{n}_m$ into the correlated noise vector $[\boldsymbol{H}^{-1}.\boldsymbol{n}_m]$. Since the elements of the noise vector $\boldsymbol{n}_m$ are independent, the covariance matrix of the correlated noise vector at the output of the ZF detector is equal to:

$$cov(\boldsymbol{H}^{-1}.\boldsymbol{n}_m) = \sigma_w^2 \boldsymbol{H}^{-1}.(\boldsymbol{H}^{-1})^H \tag{15}$$

The channel matrix $\boldsymbol{H}$ is a random matrix, and it changes each symbol period according to the previous channel assumption model. Therefore, the covariance matrix of the noise at the output of the ZF detector is random. The average of the covariance matrix in Eq. (15) is shown in Eq. (16).

$$\bar{\boldsymbol{\Phi}}_{\boldsymbol{zf}} = E\big[cov\big(\boldsymbol{H}^{-1}.\boldsymbol{n}_m\big)\big] = \sigma_w^2 \boldsymbol{Q} \tag{16}$$

$$\boldsymbol{Q} = E[\boldsymbol{H}^{-1}.(\boldsymbol{H}^{-1})^H] \tag{17}$$

$\boldsymbol{Q}$ is the correlation matrix of the inverse channel matrix $\boldsymbol{H}^{-1}$. The correlation matrix $\boldsymbol{Q}$ has N independent eigenvalues since the channel matrix $\boldsymbol{H}$ is full rank and there are $N\times N$ independent paths from the transmitting antennas to the receiving antennas. The eigenvalues of $E[\boldsymbol{H}.\boldsymbol{H}^H]$ represent the average power gains of the channel matrix in the directions of its eigenvectors, however, the eigenvalues of the $\boldsymbol{Q}$ matrix represent the average power gains of the ZF detector in the directions of its eigenvectors.

The total average power in the noise vector at the output of the ZF detector is smaller than or equal to the total average power in the noise vector at the input of the ZF detector if the rule in Eq. (18) is achieved.

$$\sum_{n=1}^{N} E\big[\lambda_{Qn}\big] \le N \tag{18}$$

λ_{Qn} is the n^{th} eigenvalue of the random matrix $[\boldsymbol{H}^{-1}.(\boldsymbol{H}^{-1})^H]$. Therefore, the ZF detector will not increase the noise power at its output as long as the condition in Eq. (18) is accomplished. For the used SDM system, the channel matrix achieves the condition in Eq. (18) if the variances of the channel gains from the transmitting antennas to the receiving antennas are greater than a certain threshold. This threshold depends on the random model of the channel. In the simulation section, this threshold is estimated for different Rayleigh channel matrices with different ranks.

4. The proposed algorithm to control channel matrix eigenvalues

At first glance, it appears that the channel gains cannot be controlled in the wireless channel, because the channel gains in wireless channel depend on the geographic distribution of the area between the transmitter and receiver. Moreover, the heights and the densities of the obstacles in the path of wave propagation affect the received signal amplitude and phase. However, if smart transmitting and receiving antennas are included in the channel model, the channel gains in the wireless channel can be controlled. Smart antennas are antenna arrays with smart signal processing algorithms used to identify spatial signal signatures such as the Direction of Arrival (DOA) of the signal and the antenna gain. Smart antennas use beamforming algorithm to create the radiation pattern of the antenna array by adding constructively the phases of the signals in the

direction of the desired receiver antenna and nulling the pattern in the direction of the undesired antennas. This can be done with a simple Finite Impulse Response (FIR) tapped delay line filter. The weights of the FIR filter may also be changed adaptively and used to provide optimal beamforming, in the sense that it reduces the Minimum Mean Square Error between the desired and actual beampattern formed.

In the used SDM system, the signal power at the inputs of the transmitting antennas is normalized. The radiation pattern of each transmitting antenna is tuned to have different gains in the direction of the receiving antennas. By the same way, the radiation pattern of each receiving antenna is tuned to have different gains in the direction of the transmitting antennas. According to the required eigenvalues for the inverse channel matrix, the gains of the transmitting antennas and the receiving antennas are adjusted to satisfy the condition in equation (18). Three scenarios may be used to adjust the gains of the transmitting and receiving antennas. In the first one, it is assumed that there is a robust feedback channel from the receiver to the transmitter, and the CSI is sent from the receiver to the transmitter through this channel. According to the CSI, the transmitter can change the gains of the transmitting antennas to minimize the cost function $\mathcal{C}$ in Eq. (19).

$$\mathcal{C} = \min_{G_t} \left| \sum_{n=1}^{N} E\left[\lambda_{Qn}\right] - (N - \epsilon) \right|^2 \quad (19)$$

G_t is the vector of transmitting antennas gains. ϵ is an arbitrary-small positive number. The vector G_t of the transmitting antenna gains affects the values of the elements in the channel matrix $\boldsymbol{H}$ in Eq. (17), which will also affect the eigenvalues λ_{Qn} of the inverse channel matrix. The gains of the transmitting antennas are adjusted to make the summation of the average eigenvalues of the inverse channel matrix smaller than or equal to the rank of the channel matrix.

In the second scenario, it is assumed that the transmitting antennas gains are different and fixed and the receiver will adjust the radiation gains of the receiving antennas to minimize the cost function $\mathcal{C}$ in Eq. (20).

$$\mathcal{C} = \min_{G_r} \left| \sum_{n=1}^{N} E\left[\lambda_{Qn}\right] - (N - \epsilon) \right|^2 \quad (20)$$

G_r is the vector of receiving antennas gains. The gains vector G_r will also affect the elements of the channel matrix $\boldsymbol{H}$ and the eigenvalues of the inverse channel matrix. By adjusting the gains of the receiving antennas according to Eq. (20), the sum of the average eigenvalues of the inverse channel matrix will be smaller than the rank of the channel matrix.

In the last scenario, the gains of the transmitting antennas and the receiving antennas are adjusted together to minimize the cost function in Eq. (21).

$$\mathcal{C} = \min_{G_t, G_r} \left| \sum_{n=1}^{N} E\left[\lambda_{Qn}\right] - (N - \epsilon) \right|^2 \quad (21)$$

After adjusting the gains of the transmitting and receiving antennas according to one of the previous three scenarios, the eigenvalues of the inverse channel matrix will be very close to the condition Eq. (18) of the eigenvalues' theory. In this case, the ZF detector will not enhance the received noise power and its performance will converge close to the ML detector performance.

5. Simulations

In this section, the results of the simulations and the implementation of the reviewed idea are presented. This section is divided into three parts. The simulations of the eigenvalues theorem are presented in the first part. However, a complete SDM system is simulated in the second part. The simulated SDM receiver uses the ZF detector to remove the interference among the received symbols. In the last part, a real-time SDM system is implemented and tested. The real-time SDM system is implemented using Xilinx FPGA kit. The ZF detector is also used in the receiver of the implemented SDM system.

The linear mapping of random vectors is simulated and assessed using Matlab m-files. In the first simulation, a vector $\boldsymbol{x}$ of five Gaussian random variables is generated. The random variables in vector $\boldsymbol{x}$ have zero means. They are independent and have the same variances. The variances of the random variables in $\boldsymbol{x}$ are changed from 6.98 dB to 37 dB. Four different 5×5 full rank matrices are used to map the input vector $\boldsymbol{x}$ to the output vector $\boldsymbol{y}$. The sums of the eigenvalues of the correlation matrices of the first and second systems are 1.707 and 0.4822, respectively. However, the sums of the eigenvalues of the correlation matrices of the third and fourth systems are 14.3965 and 26.2839, respectively. For each system, the average power of the output vector $\boldsymbol{y}$ is calculated using 10^5 sample vectors of vector $\boldsymbol{x}$. Fig. (2) shows the relation between the average power of the input vector $\boldsymbol{x}$ and the average power of the output vector $\boldsymbol{y}$ for the used four systems.

From Fig. (2), it is observed that the first and the second linear systems reduce the power of the input vector since the eigenvalues sums of their correlation matrices are smaller than five (the rank of the used

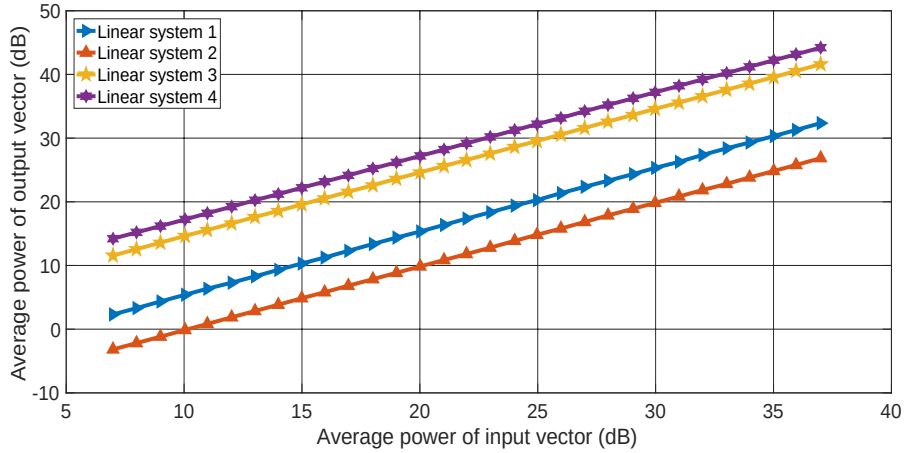

Figure. 2 The input/output average power relation for four linear systems with different correlation matrices

linear systems). However, the third and the fourth linear systems increase the power of the input vector since the eigenvalues sums of their correlation matrices are greater than five. This observation confirms the contribution of the eigenvalues' theorem. According to Eq. (10), the power gain of the linear system is equal to the trace of its correlation matrix divided by its rank. The power gains of the first and second systems are -4.6674 dB and -10.1571 dB, respectively. On the other hand, the power gains of the third and fourth systems are 4.5929 dB and 7.2072 dB, respectively.

In the next simulation, the performance of a random linear system is evaluated. Two different input vectors $\boldsymbol{x}_1$ and $\boldsymbol{x}_2$ are used in this simulation. Each vector consists of five independent Gaussian random variables with zero means. The average power of $\boldsymbol{x}_1$ is 0 dB and the average power of $\boldsymbol{x}_2$ is 10 dB. The random system is a 5×5 zero-mean Rayleigh random matrix ($\mathbf{A}$). 10^5 different input vectors of $\boldsymbol{x}_1$ and $\boldsymbol{x}_2$ are used in the simulation. The system matrix $\mathbf{A}$ is randomly changed with each input vector. There are 10^5 random Rayleigh matrices affect the elements of the input vectors at each time the simulation is done. The vectors $\boldsymbol{y}_1$ and $\boldsymbol{y}_2$ are the output vectors from the random system $\mathbf{A}$ due to the input vector $\boldsymbol{x}_1$ and $\boldsymbol{x}_2$, respectively. The average powers of $\boldsymbol{y}_1$ and $\boldsymbol{y}_2$ are calculated for each input of $\boldsymbol{x}_1$ and $\boldsymbol{x}_2$. According to the eigenvalues' theorem and Eqs. (11) and (14), the average eigenvalue (AEV) of the five random eigenvalues of the correlation matrix $E[\mathbf{A}\,\mathbf{A}^H]$ is calculated. Moreover, the sum of the five average eigenvalues (SAEVs) of the correlation matrix $E[\mathbf{A}\,\mathbf{A}^H]$ is calculated at each time the simulation is done. The previous simulation and calculations are repeated 30 times. In each time, the variances of the elements of matrix $\mathbf{A}$ are changed to have different values of the AEV of the correlation matrix $E[\mathbf{A}\,\mathbf{A}^H]$. The 10^5 Rayleigh random matrices, which affect the input vectors, are also changed each time the simulation is repeated. Fig. 3 shows the relation between the SAEVs of the correlation matrix $E[\mathbf{A}\,\mathbf{A}^H]$ versus its AEV. The average power of the output vectors from the random system $\mathbf{A}$ is calculated and displayed in Fig. 3. According to Eq. (14), the rank threshold of the sum of the eigenvalues averages of the correlation matrix $E[\mathbf{A}\,\mathbf{A}^H]$ is 6.9897 dB. It is also shown in Fig. 3.

In Fig. 3, the threshold boundary is specified. It is the vertical line at the intersection point between the rank threshold line and the line of the SAEVs of the correlation matrix $E[\mathbf{A}\,\mathbf{A}^H]$. It is observed that the average power of the output vectors from the random system $\mathbf{A}$ on the left-hand side of the threshold boundary is smaller than the average power of the input vectors. However, on the right-hand side of the boundary, the average power of the output vectors is greater than the average power of the input vectors. In other words, the average power of the output vector from the random system $\mathbf{A}$ is smaller than the average power of its input vector as long as the SAEVs of the correlation matrix $E[\mathbf{A}\,\mathbf{A}^H]$ is smaller than the rank threshold (6.9897 dB), and vice versa. This observation confirms the contribution of the eigenvalues' theorem. In the last simulation of this part, the performance of the ZF detector is evaluated individually with noise vectors. In the ZF detector, the linear mapping is done using the inverse of the channel matrix. Since the channel matrix is often a Rayleigh matrix, the linear mapping in the ZF detector is done using the inverse of a Rayleigh matrix.

The parameters of the previous simulations are repeated in this simulation except that the mapping process is done using the inverse matrix $\mathbf{A}^{-1}$. The average powers of the output vectors and the SAEVs of the correlation matrix $E[\mathbf{A}^{-1}(\mathbf{A}^{-1})^H]$ are calculated and represented in Fig. 4. The calculated

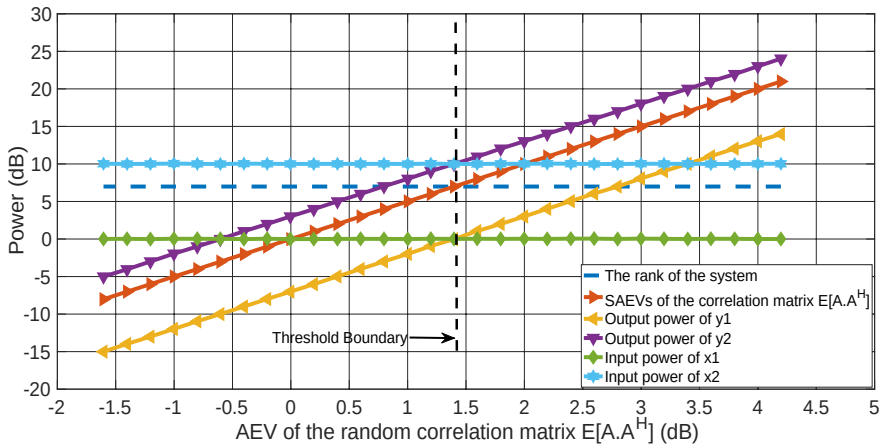

Figure. 3 The input/output average power relation for a random linear system with two different input vectors $\boldsymbol{x}_1$ and $\boldsymbol{x}_2$

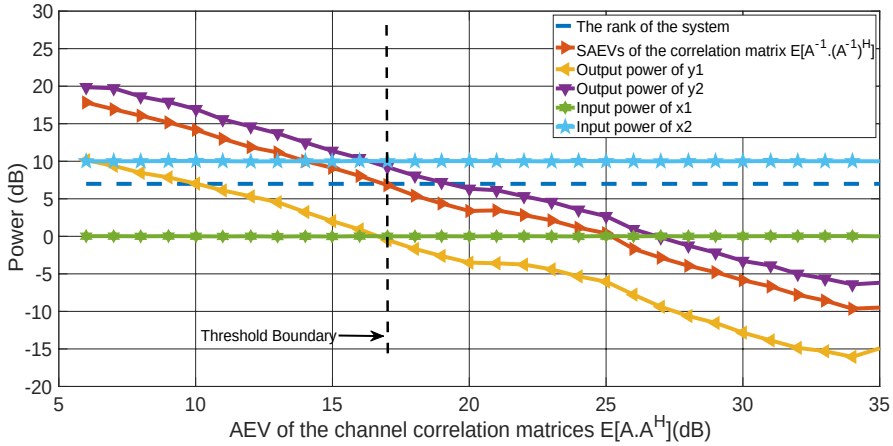

Figure. 4 The input/output average power relation for the ZF detector with two different input vectors $\boldsymbol{x}_1$ and $\boldsymbol{x}_2$

parameters are shown versus the AEV of the correlation matrix $E[\mathbf{A}\mathbf{A}^H]$.

From Fig. 4, it is observed that the average output powers and the SAEVs of the correlation matrix $E[\mathbf{A}^{-1}(\mathbf{A}^{-1})^H]$ are inversely proportional with the AEV of the channel correlation matrix $E[\mathbf{A}\mathbf{A}^H]$. This is opposite of what happened in the previous simulation because the mapping process in the ZF detector is done using the inverse of the random Rayleigh matrix $\mathbf{A}$. The threshold boundary is also specified in Fig. 4. It is observed that the average power of the output vectors from the ZF detector on the right-hand side of the threshold boundary is smaller than the average power of its input vectors. However, on the left-hand side of the boundary, the average power of the output vectors is greater than the average power of the input vectors. Hence, the average power of the output of ZF detector is smaller than the average power of its input as long as the SAEVs of the correlation matrix $E[\mathbf{A}^{-1}(\mathbf{A}^{-1})^H]$ is smaller than the rank threshold (6.9897 dB), and vice versa.

From Fig. 4, a very important conclusion is noted. As long as the AEV of the correlation matrix $E[\mathbf{A}\mathbf{A}^H]$ of the used Rayleigh matrix is greater than 17.6 dB, the ZF detector will not increase the power of the input noise vector. This conclusion does not depend on the power of the noise vector. It depends only on the eigenvalues of the correlation matrix $E[\mathbf{A}\mathbf{A}^H]$. The AEV of the correlation matrix of the Rayleigh channel in real communications systems is always less than the AEV of the rank threshold boundary. This is the reason behind the bad impression of the ZF detector performance. To get benefits from the previous contribution, the channel parameters, which merely affects the desired signal, should be changed to increase the AEV of the channel correlation matrix. For example, the gains of the transmitting antennas or the receiving antennas are adjusted to make the AEV of the correlation matrix of the Rayleigh channel greater than the AEV of the threshold boundary. Table 1 lists the estimations of the AEV of the threshold boundary for different Rayleigh channel matrices with different ranks.

The values of the AEV in Table 1 are determined from the simulations with an estimation error around ±1 dB. They may be used as a rough guide in designing SDM systems with ZF detectors. For

Table 1. The estimations of the AEV of the threshold boundary for rayleigh channel correlation matrix at different matrix ranks

The rank of Rayleigh channel matrix	The average eigenvalue of the threshold boundary
2	13 dB
3	15.1 dB
4	16.2 dB
5	17.6 dB
6	18.5 dB
7	19 dB
8	19.3 dB

Table 2. The AEV of the correlation matrices of the simulated rayleigh channels and the SAEVs of the correlation matrices of their inverse

Channel matrix	The AEV of the channel correlation matrix	The SAEVs of the inverse channel correlation matrix
Group 1	4 dB	18.87 dB
Group 2	17 dB	6.13 dB
Group 3	30 dB	-7.42 dB

accurate calculations of the AEV values, the probability density function (pdf) of the eigenvalues of the channel correlation matrix $E[\mathbf{A}\mathbf{A}^H]$ and the pdf of the SAEVs of the correlation matrix $E[\mathbf{A}^{-1}(\mathbf{A}^{-1})^H]$ need to be determined. This is not an easy task. This problem may be studied in detail in aseparate work to reduce prolongation in this article.

In the second part of the simulations, the performance of an SDM receiver with ZF detector is evaluated. The simulated SDM system uses 4 transmitting antennas and 4 receiving antennas. The used modulation scheme is 16-QAM (Quadrature Amplitude Modulation). The coherence bandwidth of the Rayleigh channel is 6 MHz. The bandwidth of the transmitted signal is 5 MHz. The transmission bit rate in the simulated SDM system is 40 Mbit/s. However, the transmission bit rate in the corresponding non-multiplexing system is 10 Mbit/s. The receiver uses a ZF detector to remove interference among the received symbols. The AEV of the channel correlation matrix and the SAEVs of the inverse channel correlation matrix are calculated. The AEV

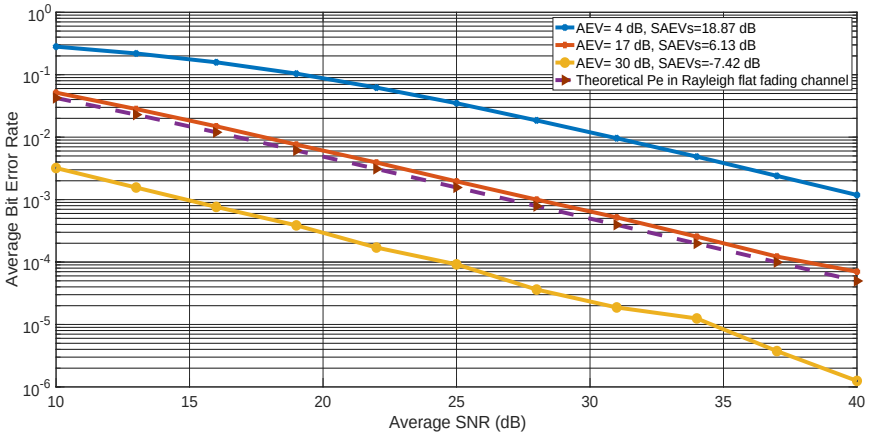

Figure. 5 The BER performance of SDM receiver with ZF detector at different matrices of rayleigh flat fading channels

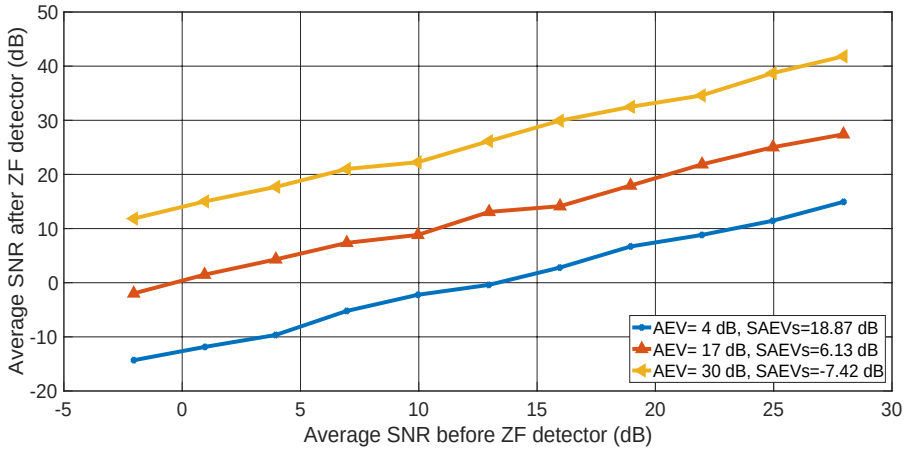

Figure. 6 A comparison between the SNR before and after ZF detector in SDM receiver at different matrices of rayleigh flat fading channels

represents the average power gain of the channel. However, the SAEVs of the inverse channel correlation matrix divided by the rank of the channel matrix (*N*) represents the total power gain of the ZF detector. According to the used channel model, the channel matrix changes randomly every symbol period T_s. Table 2 shows the values of AEV and SAEVs for three different groups of channels matrices.

The simulation is repeated three times for the three different channels groups in Table 2. The signal to interference ratio (SIR) at each receiving antenna is -4.77 dB. SIR is the ratio between signal power and interference power. The average received SNR is changed from 10 dB to 40 dB. SNR is the ratio between signal power and noise power. Fig. 5 shows the Bit-Error-Rate (BER) performance of the simulated SDM system at each value of the average received SNR. The BER is the ratio between the number of bit errors in the received data and the total number of received bits. The calculated BER is compared with the theoretical probability of error of the 16-QAM system in Rayleigh flat fading channel. According to the introduced eigenvalues theorems, the rank of the channel matrix is 6 dB.

From Fig. 5, it is observed that the optimum performance of the simulated SDM receiver is achieved when the SAEVs of the inverse channel correlation matrix is equal to the rank of the channel matrix (6 dB). In this case, the total average power gain of the ZF detector is approximately 0 dB. This happens with the second group of channel matrices, at which the average power gain of the channel is approximately 17 dB. Since the real flat fading channel is passive, the channel gain is achieved in real systems by increasing the power amplifiers gains in the transmitter or changing the gains of the transmitting antennas and the receiving antennas.

When the average channel gain increases more than 17 dB, the BER performance of the ZF detector is enhanced because the SAEVs of the inverse channel correlation matrix is smaller than the rank of the channel matrix. This enhancement does not depend on the received SNR. This is observed in the simulation with the third group of channels. The

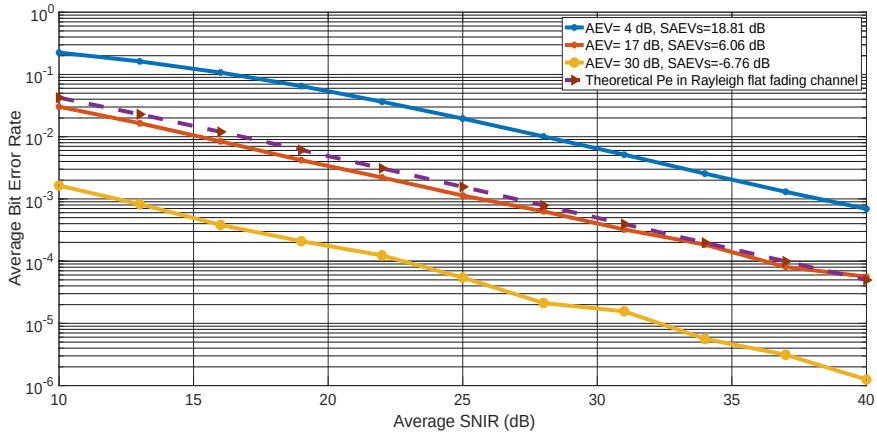

Figure. 7 The BER performance of the SDM receiver with ZF detector versus the received SNIR at different matrices of rayleigh flat fading channels

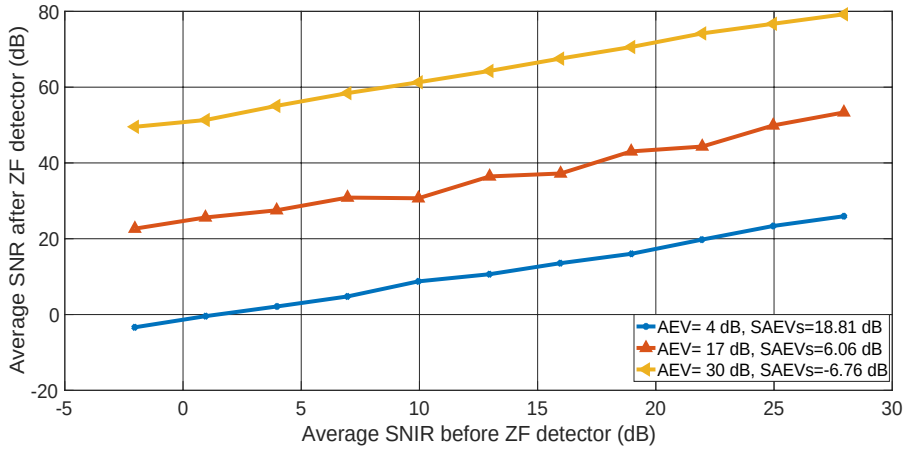

Figure. 8 A comparison between the SNIR before ZF detector and SNR after ZF detector in SDM receiver at different matrices of rayleigh flat fading channels

Table 3. Synthesis results of the implemented SDM system

Resource	Available	Transmitter	Receiver	Utilization %
LUT	303600	55324	125179	59.45
FF	607200	82331	180844	43.34
IO	700	24	24	6.8
BUFG	32	5	7	37.5
Worst negative slack		0.832 ns	0.087 ns	
Worst hold slack		0.042 ns	0.035 ns	

SAEVs is approximately 13.5 dB lower than the rank threshold. The BER performance of the SDM system with the third channel group is 13 dB better than the theoretical probability of error of 16-QAM systems, whatever the received SNR is.

This performance enhancement is not due to the increase in the received SNR since the BER is calculated at the same values of the SNRs used with the second group of channels. However, the performance enhancement is due to that the ZF detector will reduce noise power at its output to be smaller than the noise power at its input when the SAEVs is smaller than the rank.

Finally, when the first group of the channel matrix is used in the simulation, it gives the worst BER

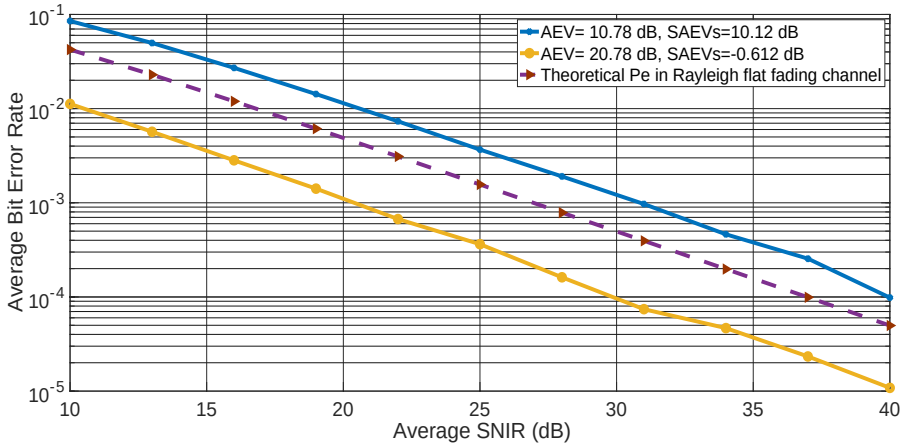

Figure. 9 The BER performance of real-time SDM system with ZF detector versus the received SNIR at different matrices of rayleigh flat fading channels

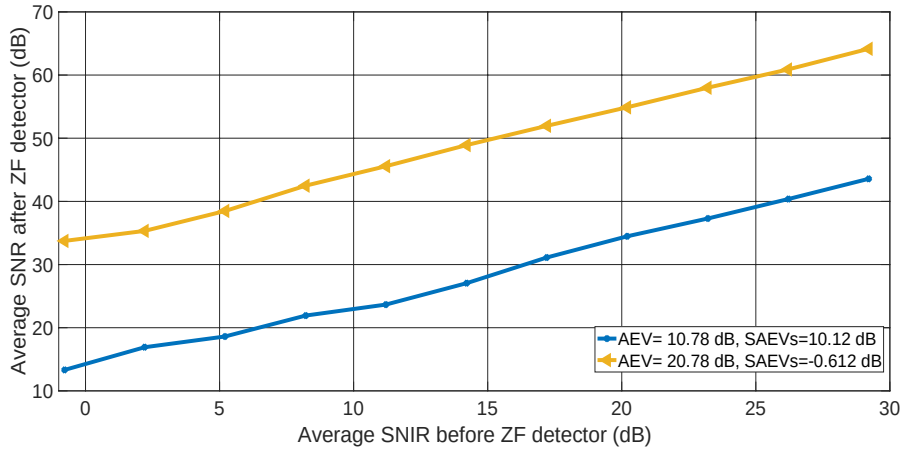

Figure. 10 A comparison between the SNIR before ZF detector and SNR after ZF detector in real-time SDM receiver at different matrices of rayleigh flat fading channel

performance because the SAEVs is bigger than the rank threshold of the channel matrix. In this case, the ZF detector enhances the noise power at its outputs. The SNR at the input of the baseband detector is smaller than the SNR at the input of the baseband detector of the previous two cases. This is the reason for the bad BER performance of the ZF detector when the first group of the channel matrix is used.

Fig. 6 displays the average SNR at the output of the ZF detector versus the average SNR at its input for the previous three channels groups. The figure confirms the aforementioned contributions. The average SNR at the output of the ZF detector changes for the same SNR at its input according to the used channel group. The average SNR at the output of the ZF detector is bigger than the average SNR at its input as long as the SAEVs of the inverse channel correlation matrix is smaller than the rank threshold. This is the reason why the BER performance is better in the case of the third channel group than the other cases.

The previous simulation is repeated but the average BER is displayed versus the average received Signal to Noise and Interference Ratio (SNIR) at each receiving antenna. Fig. 7 shows the average BER versus the average SNIR and Fig. 8 shows the average SNR at the output of the ZF detector versus the average SNIR at its input. The same observations are contributions are achieved for this simulation.

Therefore, the BER performance of the ZF detector neither depends on the received noise power nor the received interference power, but it depends on the eigenvalues of the correlation matrix of the inverse channel matrix.

In the last part of this section, a real-time implementation of the simulated SDM system is tested with a practical Rayleigh channel. Xilinx FPGA kit is used to implement the SDM transmitter and receiver. The used FPGA platform is Virtex-7 VC707. Table 2. lists the synthesis results of the implemented SDM system.

A file of 1 G bits is transmitted with a rate of 30 M bits/s. The carrier frequency of the transmitted signal is 5 GHz. 3 transmitting antennas and 3 receiving antennas are used in the implemented system. The spacing between the antennas is 30 cm. According to the eigenvalues' theorems, the rank threshold of the channel matrix is 4.77 dB. From Table 2, the average channel gain should be greater than 15.1 dB to use ZF detector in the receiver without any noise enhancement. The power amplifiers and the gains of the transmitting antennas and receiving antennas are considered as a part of the channel matrix. The gains of the power amplifiers, the transmitting antennas, and receiving antennas are adjusted to get two different channel matrices with AEV of 10.78 dB and 20.78 dB. The received average SNIR is changed from 20 dB to 35 dB. The average BER is calculated and displayed in Fig. 9 using the previous two channels.

Form Fig. 9, it is observed that the average BER is changed for the same received SNIR according to the value of the AEV of the channel matrix. When the AEV is bigger than 15.1 dB, the average BER is smaller than the BER when the AEV is smaller than15.1 dB. The SAEVs in the second case is smaller than the rank threshold of 4.77 dB. However, the SAEVs in the first case is bigger than the rank threshold.

Therefore, the performance of the ZF detector is not affected with the received SNIR but it is affected with the AEV of the channel correlation matrix and the SAEVs of the inverse channel correlation matrix. The AEV of the channel correlation matrix can be controlled by the power amplifiers gains in the transmitter, the gains of the transmitting antennas and the gains of the receiving antennas. Fig. 10 display the average SNR at the output of the ZF detector versus the average SNIR at its input. The average SNR at the output of the ZF detector is smaller than the Average SNR at its input as long as the SAEVs of the correlation matrix of the ZF detector mapping matrix is smaller than the rank threshold, and vice versa.

6. Conclusions

SDM system increases the data transmission rate by sending the modulated symbols parallel using different transmitting antennas. SDM system sends the modulated symbols in the same bandwidth, which is used by the non-multiplexing system. The bandwidth efficiency of the SDM system is greater than the bandwidth efficiency of any other multiplexing system. The channel model of the SDM system is conserved as a flat fading channel to prevent ISI among the received symbols. This is accomplished by reducing the transmission rate of each transmitting antenna to get a transmission bandwidth smaller than the coherence bandwidth of the channel. In the same time, the number of the transmitting antennas is increased to achieve the required high transmission rate.

In the used SDM receiver, ZF detector is used after the matched filters to remove interferences among the multiplexed symbols because its complexity changes linearly with the number of the interfering symbols. The random variables in the noise vector after the matched filters in the SDM receiver are independent and have the same

probability distribution functions. The noise performance of the ZF detector does not depend on the received SNR. The eigenvalues of the correlation matrix of the ZF detector-mapping matrix and the rank of this mapping matrix are the parameters, which control the performance of the ZF detector. The channel noise power at the outputs of the ZF detector increases or decreases according to the relation between the sum of the eigenvalues of the correlation matrix of the ZF detector and the rank of its mapping matrix. If the sum of these eigenvalues is greater than the rank of the mapping matrix, the ZF detector will enhance the channel noise power at its output and the BER will increase at the output of the baseband detector. However, if the sum of these eigenvalues is equal to the mapping matrix rank, the ZF detector will not enhance the noise power at its output and the BER performance of the ZF detector will be closed to the BER performance of the ML detector. Moreover, the ZF detector will reduce the channel noise power at its output if the sum of these eigenvalues is smaller than the mapping matrix rank.

Since the mapping matrix of the ZF detector is the inverse of the channel matrix, there is a relation between the average eigenvalue of the channel correlation matrix and the sum of the eigenvalues of the correlation matrix of the ZF detector-mapping matrix. Simulation results show that the ZF detector will not increase the noise power at its outputs if the average eigenvalue of the channel correlation matrix is greater than a certain threshold. The results of the simulations give estimations for this threshold for different ranks of channel matrices. According to the used mathematical model, the elements of the channel matrix depend on the transmitting antennas gains and the receiving antennas gains. By adjusting these gains, the average eigenvalue of the channel matrix can be greater than the estimated threshold. In this case, the ZF detector reduces the power of the channel noise whatever its input SNR is high or low. The noise performance of the ZF detector does not depend on the received SNR, but it depends on the average eigenvalue of the channel correlation matrix. The output SNR at the output of the ZF detectors changes according to the average eigenvalue of the correlation matrix at the same input SNR.

In future work, the probability distribution of the average eigenvalue of the channel correlation matrix and the probability distribution of the sum of the eigenvalues of the ZF detector correlation matrix will be determined. A mathematical equation, which gives the estimation of the average eigenvalue threshold of the channel matrix, will also be specified.

Declaration of interests

The authors declare no conflict of interest.

Author Contributions

"Conceptualization, A. Y. Hassan; methodology, A. Y. Hassan; software, A. Y. Hassan and Ali Saleh; validation, A. Y. Hassan and Ali Saleh; formal analysis, A. Y. Hassan; investigation, A. Y. Hassan and Ali Saleh; resources, A. Y. Hassan; data curation, Ali Saleh; writing—original draft preparation, A. Y. Hassan —review and editing, A. Y. Hassan and Ali Saleh; visualization, A. Y. Hassan; supervision, A. Y. Hassan; project administration, A. Y. Hassan; funding acquisition, A. Y. Hassan.

References

[1] J. Choi, Y. Nam, and N. Lee, "Spatial Lattice Modulation for MIMO Systems", *IEEE Transactions on Signal Processing*, Vol. 66, No. 12, pp. 3185-3198, 2018.

[2] S. Gao, X. Cheng, and L. Yang, "Spatial Multiplexing with Limited RF Chains: Generalized Beamspace Modulation (GBM) for mmWave Massive MIMO", *IEEE Journal on Selected Areas in Communications*, Vol. 37, No. 9, pp. 2029-2039, 2019.

[3] X. Liu and I. Darwazeh, "Doubling the Rate of Spectrally Efficient FDM Systems Using Hilbert Pulse Pairs", In: *Proc. of* 26*th International Conf. on Telecommunications (ICT)*, Hanoi, Vietnam, pp. 192-196, 2019.

[4] U. Choudhary and V. Janyani, "Bandwidth efficient frame structures for flip OFDM with phase conjugated sub carriers and LDPC encoding", *Optik*, Vol. 204, 2020.

[5] Z. Wang, L. Zheng, J. Chen, M. Lin, and X. Deng, "MIMO-MFSK Spatial Multiplexing in Rician Channel with Large Doppler Shift", In: *Proc. of IEEE 19th International Conf. on Communication Technology (ICCT)*, Xi'an, China, pp. 649-652, 2019.

[6] A. Udawat and S. Katiyal, "Signal detection techniques for spatially multiplexed MIMO systems", In*: Proc. of 6th International Conf. on Computing for Sustainable Global Development*, New Delhi, India, p 432-434, 2019.

[7] T. S. Rappaport, *Wireless Communications: Principles and Practice*, Prentice Hall, 2nd edition, 2002.

[8] A. Y. Hassan, "Minimizing the Effects of Inter-Carrier Interference Signal in OFDM System Using FT-MLE Based Algorithm", *Wireless*

Personal Communications, Springer, Vol. 97, No. 2, pp 1997–2015, 2017.

[9] A. Y. Hassan, "A Novel Structure of High Speed OFDM Receiver to Overcome ISI and ICI in Rayleigh Fading Channel", *Wireless Personal Communications, Springer*, Vol. 97, No. 3, pp 4305–4325, 2017.

[10] S. Birgmeier and N. Goertz, "Approximate Message Passing for Joint Activity Detection and Decoding in Non-orthogonal CDMA", In*: Proc. of* 23*rd International ITG Workshop on Smart Antennas*, Vienna, Austria, pp. 1-5, 2019.

[11] Y. Liu, W. Zhang, and P. C. Ching, "Time-reversal space–time codes in asynchronous two-way relay networks", *IEEE Transactions on Wireless Communication*, Vol. 15, No. 3, pp. 1729-1741, 2016.

[12] W. Tang, S. Yang, and X. Li, "Implementation of Space-time Coding and Decoding Algorithms for MIMO Communication System Based on DSP and FPGA", In*: Proc. of IEEE International Conf. on Signal Processing, Communications and Computing (ICSPCC)*, Dalian, China, pp. 1-5, 2019.

[13] I. Ahn, J. Kim, and H. Song, "Adaptive Analog Self-Interference Cancellation for In-band Full-Duplex Wireless Communication", In*: Proc. of IEEE Asia-Pacific Microwave Conf. (APMC)*, Marina Bay Sands, Singapore, pp. 414-416, 2019.

[14] P. Herath, A. Haghighat, and L. Canonne-Velasquez, "A Low-Complexity Interference Cancellation Approach for NOMA", In*: Proc. of IEEE 91st Vehicular Technology Conf. (VTC2020-Spring)*, Antwerp, Belgium, pp. 1-5, 2020.

[15] M. Gao, L. Zhang, C. Han, and J. Ge, "Low-Complexity Detection Schemes for QOSTBC with Four-Transmit-Antenna", *IEEE Communications Letters*, Vol. 19, No. 6, pp. 1053-1056, 2015.

[16] S. Verdu, "Multiuser Detection", Cambridge press, U.K, 1998.

[17] Y. Hama and H. Ochiai, "A low-complexity matched filter detector with parallel interference cancellation for massive MIMO systems", In*: Proc. of IEEE 12th International Conf. on Wireless and Mobile Computing, Networking and Communications (WiMob)*, New York, United State, pp. 1-6, 2016.

[18] J. GuEmaila and R. Lamare, "Joint interference cancellation and relay selection algorithms based on greedy techniques for cooperative DS-CDMA systems", *EURASIP Journal on Wireless Communications and Networking*, Vol. 59, pp. 1-19, 2016.

[19] L. Fang, L. Xu, and D. Huang, "Low Complexity Iterative MMSE-PIC Detection for Medium-Size Massive MIMO", *IEEE Wireless Communications Letters*, Vol. 5, No. 1, pp. 108-111, 2016.

[20] B. Ling, C. Dong, J. Dai, and J. Lin, "Multiple Decision Aided Successive Interference Cancellation Receiver for NOMA Systems", *IEEE Wireless Communications Letters*, Vol. 6, No. 4, pp. 498-501, 2017.

[21] F. Uddin and S. Mahmud, "Carrier Sensing-Based Medium Access Control Protocol for WLANs Exploiting Successive Interference Cancellation", *IEEE Transactions on Wireless Communications*, Vol. 16, No. 6, pp. 4120-4135, 2017.

[22] M. Mandloi, M. Hussain, and V. Bhatia, "Improved multiple feedback successive interference cancellation algorithms for near-optimal MIMO detection", *IET Communications*, Vol. 11, No. 1, pp. 150-159,2017.

[23] R. Fischer, C. Stierstorfer, and R. Mueller, "Subspace Projection and Noncoherent Equalization in Multi-User Massive MIMO Systems", In*: Proc. of 10th International ITG Conf. on Systems, Communications and Coding*, Hamburg, Germany, pp. 1-6, 2015

[24] S. Şahin, A. M. Cipriano, C. Poulliat, and M. Boucheret, "Iterative Equalization with Decision Feedback Based on Expectation Propagation", *IEEE Transactions on Communications*, Vol. 66, No. 10, pp. 4473-4487, 2018.

[25] C. Dong, K. Niu, and J. Lin, "An Ordered Successive Interference Cancellation Detector with Soft Detection Feedback in IDMA Transmission", *IEEE Access*, Vol. 6, pp. 8161-8172, 2018.

[26] J. Minango, C. Altamirano, and C. Almeida, "Performance difference between zero-forcing and maximum likelihood detectors in massive MIMO systems", *Electronics Letters*, Vol. 54, No. 25, pp. 1464-1466, 2018.

[27] S. Hu and E. Leitinger, "Joint Modulus Zero-Forcing MIMO Detector", In*: Proc. of IEEE Wireless Communications and Networking Conf. (WCNC)*, Marrakesh, Morocco, pp. 1-5, 2019.

[28] J.G. Proakis, *Digital communications*, New York: McGraw-Hill, 2001.

[29] Y. Khattabi and M. Matalgah, "Improved error performance ZFSTD for high mobility relay-

based cooperative systems", *Electronics Letters*, Vol. 52, No. 4, pp. 323-325, 2016

[30] H. Q. Ngo, M. Matthaiou, T. Q. Duong, and E. G. Larsson, "Uplink Performance Analysis of Multicell MU-SIMO Systems with ZF Receivers", *IEEE Transactions on Vehicular Technology*, Vol. 62, No. 9, pp. 4471-4483, 2013.

[31] E. Guerrero, G. Tello, and F. Yang, "Simulation and performance analysis for ordering algorithm in ZF and MMSE detectors for V-BLAST architectures", In*: Proc. of International Conf. on Computer Science and Network Technology*, Harbin, United State, pp. 59-64, 2011.